Available online at www.sciencedirect.com

ScienceDirect

Physics Procedia 77 (2015) 42 – 49

Physics Procedia

International Conference on Laser Applications at Accelerators, LA3NET 2015

Stability and resolution studies of HOMBPMs for the 1.3 GHz superconducting accelerating cavities at FLASH

L. Shi* [a,b], N. Baboi [a], and R.M. Jones [b]

[a] DESY, Notkestr. 85, 22607 Hamburg, Germany
[b] School of Physics and Astronomy, The University of Manchester, Oxford road, Manchester, M13 9PL, UK

Abstract

HOMBPMs (HOM based Beam Position Monitors) are installed at the FLASH facility at DESY, Hamburg. These are aimed at aligning the beam and monitoring the beam position. Over time, the accuracy of beam position prediction is degraded. This is due to instability issues in the 1.3 GHz and 3.9 GHz superconducting cavities and associated electronics. In this paper, we demonstrate for the first time a measurement technique which is stable and can be relied upon over a period of three months with unprecedented resolution (below 4 μm horizontally and 2 μm vertically). We attribute this improvement in stability to a focused campaign on various signal processing and analysis techniques. These techniques include SVD (Singular Value Decomposition), ANN (Artificial Neural Network) and PLS (Partial Least Square). We found the best resolution and computational power using the latter method, PLS. These techniques are directly applicable to the HOMBPM system at the European XFEL that is currently under construction. However, they are in many ways generic and hence applicable to other measurement methods.

Peer-review under responsibility of the University of Liverpool

Keywords: BPM, HOM, HOMBPM, PLS, SVD, ANN, RMS error, resolution, superconducting accelerating cavity

1. Introduction

FLASH (Free-electron-LASer in Hamburg) is a user facility to generate XUV and soft X-ray pulses by the SASE (Self Amplified Spontaneous Emission) process from energetic electron beam bunches [1]. Along the linac, there are seven accelerating cryo-modules. Each of them contains eight superconducting TESLA cavities [2]

* liangliang.shi@desy.de

Peer-review under responsibility of the University of Liverpool
doi:10.1016/j.phpro.2015.11.008

working at 1.3 GHz. One module with four 3.9 GHz cavities is used to linearize the energy spread [3]. Each cavity has two HOM (Higher Order Mode) couplers to extract the beam excited electromagnetic fields (wakefields). HOMBPMs (HOM based Beam Position Monitors) for both 1.3 GHz and 3.9 GHz cavities at FLASH have been designed [4][6] based on dipole modes.

The HOMBPMs can predict the beam position with good resolution [4]. However, the beam position readouts, after careful calibration, drift away over a day or so for both the 1.3 and 3.9 GHz cavities. This instability impedes its reliable application as a BPM. Currently the HOMBPM system can only be routinely used as a dipole power meter to optimize the beam orbit and therefore reduce the effects of the transverse wakefields. This paper presents studies to mitigate the instability in 1.3 GHz cavities. To this end, we developed several methods to stabilize the HOMBPM measurements. Because the HOM couplers are not designed for BPM application, data analysis has proved to be more difficult than for a standard cavity BPM. Therefore, we mainly focus on model independent analysis to extract the beam position.

In section 2, a brief overview of wakefields and Higher Order Modes is given. Then the basic principle of a HOMBPM is explained. Section 3 deals with the data pre-processing and signal processing, a necessary step for calibration. The analysis and results are described in section 4. A conclusion and outlook ends the paper in section 5.

2. The principle of a HOMBPM

2.1. Higher Order Modes and dipole signal

When a bunch of electrons traverses a cavity, wakefields are excited. The wakefields can be decomposed into various modes (resonances), classified into ‘monopole’, ‘dipole’ etc. [6]. The modes with higher resonant frequencies than the accelerating mode are referred as Higher Order Modes (HOMs).

HOMs can potentially cause beam emittance dilution or beam break up etc. [7]. Special HOM couplers were installed to damp the long range wakefields that affect the subsequent bunches. When the bunch offset is relatively small, the transverse wakefields are dominated by dipole modes [8]. These dipole modes are themselves restricted to a series of bands, and each component presents a transverse momentum kick to the beam [9]. Here we focus on those with the largest kick factors as only these are likely to produce sufficiently large radiation to the attached HOM couplers.

The dipole signal from the HOM ports can result from a combination of a bunch offset, tilt, or an angle [10]. Normalized with bunch charge, the signal induced is proportional to the bunch offset or angle (either tilt or angle) for small angles. The formulas for bunch offset, tilt and the angle in [10] suggest that at FLASH the contribution of bunch tilts is vanishingly small compared with beam offset signals whilst the contribution from beam angle is not negligible [4][10]. Following the reasoning in [4], a 1 mrad signal will excite the signal that has the same amplitude as 100 μm bunch offset for 1.3 GHz cavities.

2.2. The HOMBPM measurement principle

HOMBPMs are based on the beam-excited dipole signals radiated to the HOM couplers. The 1.3 GHz cavities at FLASH have two HOM couplers to damp the wakefields [2]. These are mounted on the 78 mm beam pipes at both sides of the cavity. They span an angle of 115^{o} azimuthally in order to couple both dipole and quadrupole modes [2]. HOM signals are transferred via long cables (tens of meters) from the FLASH tunnel.

For the HOMBPM a dipole mode at around 1.7 GHz [11] was selected for beam position monitoring in the 1.3 GHz cavities since it has strong coupling to the beam. Therefore it provides higher sensitivity to the beam position monitor. The block diagram is shown in Figure 1.

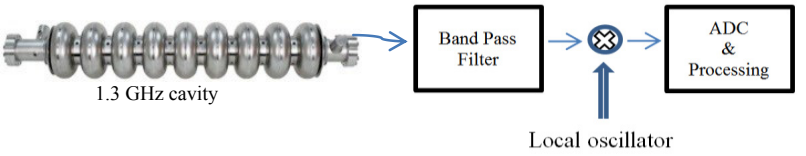

Figure 1 Block diagram of HOMBPM signal processing chain. The bandpass filter is centered at 1.7 GHz and has a bandwidth of 20 MHz. The ADC sampling clock is around 108 MHz.

The HOM signal is band filtered at 1.7 GHz with a 20 MHz bandwidth and mixed down to 20 MHz IF (intermediate frequency) signal [11]. The IF signal is then sampled at around 108 MHz and transmitted to the DOOCS control system [12]. A user defined program was developed to perform data acquisition and processing. An example of a signal and its FFT are shown in Figure 2 (red curves). The green curves will be explained in section 3.2.

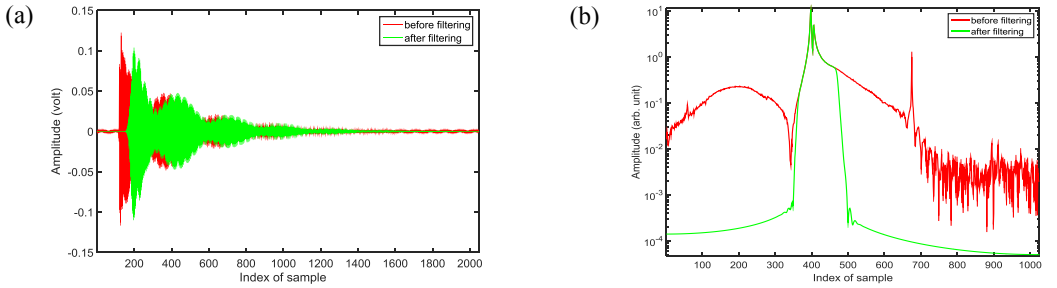

Figure 2 Example of a dipole signal before (red) and after (green) Butterworth filter in time domain (a) and frequency domain (b). Note that the filter does not refer to the one used in the electronics. It is noticeable that the noise in high frequency (index > 700 in (b)) range has been removed after filtering. The waveform is approximately 19 μs in duration. The frequency in (b) is in the range of 0-54 MHz.

3. Data preparation and signal processing

All data were recoded with a MATLAB program based on the interface provided by DOOCS. We first present the methodology used in selecting and organizing the data. The signal processing is discussed in section 3.2.

3.1. Data preparation

Signals from all 16 HOM couplers in the 5th cryo-module at FLASH were recorded, synchronously, for the same bunch. The charge was read from the nearby toroids, and the beam positions were recorded from two BPMs located upstream and downstream of the module. The measurement schematic is shown in Figure 3(a).

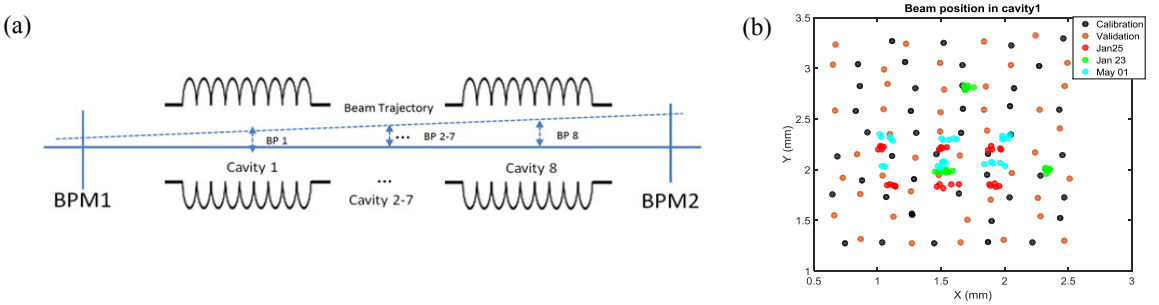

Figure 3 (a) Schematic of the measurement setup. The beam positions are recorded by BPMs 1 and 2. The beam position in each cavity can be interpolated from them. A straight beam trajectory is assumed, since the RF in the cavities and the quadrupoles between the BPMs were off. (b) Interpolated beam positions based on BPM1 and BPM2 in cavity 1 on various days.

Prior to calibrating, we carefully removed data points at which the BPMs could not work properly, or the dipole waveforms were saturated. The HOMBPMs were calibrated in an approximately 2×2 mm^2 range. They were evaluated with a different set of data from the same day (January 28, 2015). Data gathered from January 23, 25 and May 1, 2015 were used to evaluate the performance. Figure 3(b) shows the beam position interpolated in cavity 1.

The data is constructed in a matrix format,

$$D = \begin{pmatrix} data_1 \\ data_2 \\ \vdots \\ data_m \end{pmatrix} = (d_1, d_2, \dots d_n) \in R^{m \times n}, \quad (1)$$

where $data_m$ represents the m^{th} measurements. The position data is organized as:

$$P = \begin{pmatrix} x_1 & y_1 \\ x_2 & y_2 \\ \vdots & \vdots \\ x_m & y_m \end{pmatrix} \in R^{m \times 2}, \quad (2)$$

where (x_m, y_m) is the beam position interpolated from the BPMs. The process of calibration aims to find the coefficients between the data matrix *D* and the position matrix *P*. Before calibration, we need to pre-process the signal to remove components that have no correlation with the beam position.

3.2. Dipole signal processing

It was found that there was phase noise in the dipole signals. This motivates us to process the signal before any calibration. The main information is contained within the two peaks (index 350~500) in Figure 2(b). The two peaks have linear dependence on the beam position [13]. The other part of the spectrum is not relevant for beam position. We designed a 15th order Butterworth bandpass digital filter to remove the unwanted parts. The magnitude of the passband is nearly unity (0.1 dB ripple) while the stopband of the filter provides enough damping (-100 dB).

One example of dipole signal before and after filtering is shown in Figure 2. Since the following analysis does not rely on the phase information, the obvious distortion of phase in Figure 2(a) does not concern us in this paper. The filtered spectra (Figure 2(b)) were normalized with the charge and then were organized into data matrix *D*. The data was not normalized with the charge measured directly [14][4] but with the mean value from multiple measurements during each beam time. In this way, we potentially minimize the noise of the charge measurements from the toroid.

Forty-four measurements were selected for calibration from data taken on January 28. Another 44 measurements obtained on the same day were used for evaluating the calibration (called validation in this paper). Other 30, 28 and 28 measurements from January 25, 23 and May 1 were used for validation over a longer time period.

4. HOMBPM calibration and characterization

The HOMBPMs in module 5 were calibrated based on the pre-processed data as described in section 3. The first three cavities were analyzed in order to evaluate the resolution of the HOMBPM. In the following subsection the parameters used for evaluation are introduced. Then the calibration procedure based on 3 methods is described. Subsection 4.3 presents the analysis of the calibration results, while the resolution of the HOMBPMs is discussed in the last part.

4.1. RMS error and resolution

We use the RMS error as a figure of merit to assess the calibration. The RMS error is defined as the root mean square of the difference between interpolated beam positions from the two BPMs (Figure 3) and the calibrated readouts from the HOMBPMs:

$$E_{rms} = \sqrt{\frac{1}{m}\sum_{i=1}^{m}(P_i - P_i^{pre})^2}, \tag{3}$$

where P_i^{pre} is the beam position given by HOMBPM for measurement i, P_i is the interpolated beam position from the two BPMs for measurement i, and m is the number of measurements.

The HOMBPM resolution is calculated based on the 3 BPM method [10]. More specifically, beam positions given by the HOMBPM in cavity 2 were compared with beam positions from the HOMBPMs in cavity 1 and 3. The standard deviation (one sigma) of the residuals is calculated and a geometry factor $\sqrt{2/3}$ is applied [4][10]. The resolution of the HOMBPM can be obtained by:

$$R_{HOMBPM} = \sqrt{\frac{2}{3}}\sqrt{\frac{1}{m}\sum_{i=1}^{m}(P_2^H - a\cdot P_1^H - b\cdot P_3^H - c)^2}, \tag{4}$$

where $P_{1,2,3}^H$ represent the beam position measured from HOMBPM at cavities 1, 2 and 3. The coefficients a, b and c can be calculated by linear regression [10]. The HOMBPMs 1, 2, 3 are assumed to have identical resolution.

4.2. Calibration based on PLS, SVD and ANN

We have investigated 3 methods for calibration: PLS (Partial Least Square), SVD (Singular Value Decomposition) and ANN (Artificial Neural Network). The general calibration step is: 1. interpolate the beam position into each cavity and build matrix P in Eq. 2; 2. concatenate the dipole signals (spectra) from both couplers of a cavity and build matrix D (Eq. 1); 3. calculate the correlation between the matrices P and D. Written in a compact matrix form, this reads

$$D \cdot C = P, \tag{5}$$

where C is the correlation or calibration matrix that can be obtained by multiple linear regression of D against P. Each row in matrix D corresponds to one measurement, and each column corresponds to one predictor in the regression model. To alleviate the potential issue resulting from correlation among predictors, we adopted partial least square (PLS) regression [15]. In this paper, the components found by PLS methods are called latent components and they were put in the matrix D.

In the SVD method, the amplitudes of dipole signal in the SVD mode space are recorded in matrix D. Like in the PLS method, the calibration matrix can be obtained by linearly regressing D against P. A column of ones corresponding to intercept is added.

The calibration matrix C can also be represented by a neural network to map the complicated relations, if any, between D and P. To this end, we designed one feedforward neural network based on the Bayesian regulation algorithm [16][17]. We discuss the three methods in the following subsections.

4.2.1. Calibration based on PLS

In principle each sample from the spectrum (i.e. each column of D) can be treated as a single predictor in the linear regression model. However, all samples are correlated to a certain extent. This violates the assumption of independence among predictors in multiple linear regression. The model is also vulnerable to noise from measurement [14][16]. PLS regression was first developed to overcome this issue [15]. We use PLS to find latent components in the spectrum that have high correlation with the beam position.

The latent components are put in the data matrix D column wise. The linear regression of D against P is performed to find the calibration matrix C. The RMS error is calculated to evaluate the calibration. After calibration, an independent set of data from the same day is applied to validate the performance of the calibration.

The RMS error (for both calibration and validation) dependence on the number of latent components is shown in Figure 4 for cavities 1, 2 and 3.

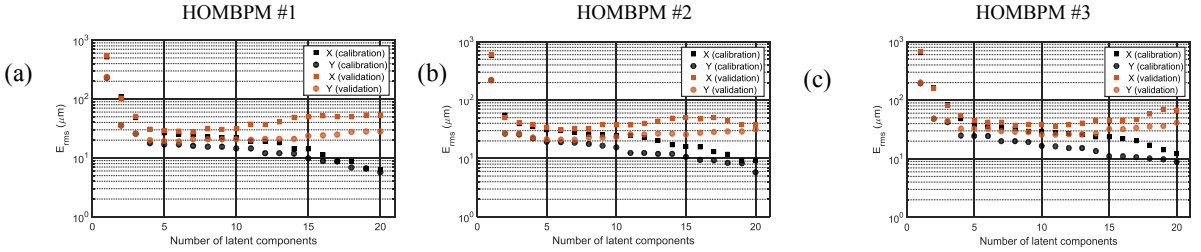

Figure 4 The RMS error dependence on the number of latent components for HOMBPMs 1, 2 and 3. Data from January 28 was used for calibration and validation.

The minimum number of latent components needed for calibration without increasing the validation RMS error is 6. Therefore, 6 latent components were used for calibration and later for resolution calculation.

4.2.2. Calibration based on SVD

In the SVD method, the spectrum matrix D is decomposed to find a number of principal components (SVD modes). These SVD modes generally contain a combination of physical modes [4]. The details of the SVD method can be found in [18][4][14].

The amplitudes for each spectrum in the SVD mode space can be calculated by the dot product:

$$A = D \cdot V = (A_1^{SVD}, A_2^{SVD}, \dots A_n^{SVD}), \tag{6}$$

where A_n^{SVD} is a vector containing amplitudes for all measurements in the n^{th} SVD mode, V is the SVD modes found by the decomposition ($D = U \cdot S \cdot V^T$).

The SVD mode amplitudes (A in Eq. 6) are put in the data matrix D column wise. The linear regression of D against P is performed to find the calibration matrix C. The RMS error is calculated to evaluate the calibration.

The RMS error (for both calibration and validation) dependence on the number of SVD modes is shown in Figure 5 for cavities 1, 2 and 3.

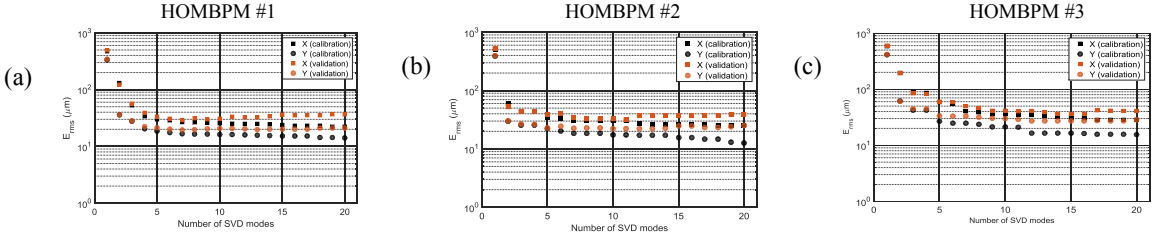

Figure 5 The RMS error dependence on the number of SVD modes for HOMBPMs 1, 2 and 3. The calibration and validation was performed on January 28, 2015.

The minimum number of SVD modes needed for calibration without increasing the validation RMS error is 7, 11, 14 for cavity 1, 2 and 3 respectively. We point out here that the number of modes chosen for calibration is somewhat arbitrary within the region where the RMS error has minor change (e.g. modes number 7-11 in Figure 5(b)). Reducing or adding a few modes has only a minor influence on the RMS error.

4.2.3. Calibration based on ANN

Artificial neural network (ANN) is a branch of statistical learning methods [19]. There is a wide range of topologies available for different purposes [17]. For the beam position extraction, we choose a feedforward neural network based on one hidden layer with 20 neurons for computation. The inputs are the amplitudes calculated in the SVD method. The interpolated beam positions were used as the outputs (targets) for learning. This forms a supervised learning problem. We build two separate networks for x and y.

The RMS error dependence on the number of inputs is shown in Figure 6 for all three cavities. The number of inputs for ANN is chosen as 4, 2 and 3 respectively, based on the criteria that there is no decrease in the RMS error for validation. From Figure 6, we can observe that generally the RMS error for validation favors the hidden layer with smaller number of inputs. The number of inputs (SVD modes) needed is smaller than in the SVD method.

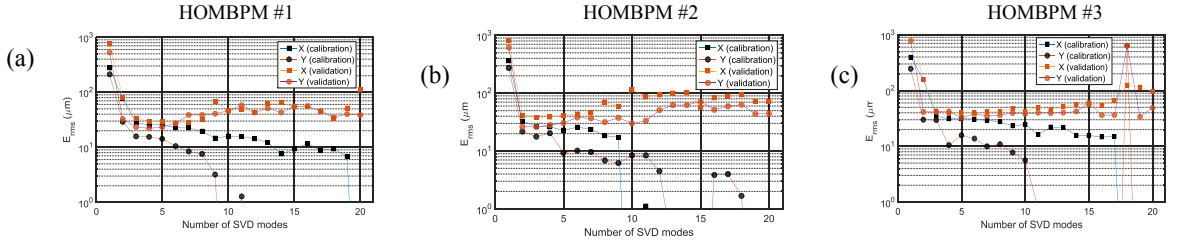

Figure 6 The RMS error dependence on the number of inputs for HOMBPMs 1, 2 and 3. The points with error below 1 μm are excluded from the plots and are regarded as over-trained by the network.

In summary, we calibrated the HOMBPM based on the methods PLS, SVD and ANN. They show comparable performance in terms of validation RMS error (~30 μm). PLS operates faster than the other two methods in general.

4.3. RMS error

Data from January 25, January 23 and May 1, 2015, were used to track the performance of the calibrated HOMBPMs. The RMS error is around 50 μm for all methods.

Several factors contribute to the RMS error: 1. the resolution of the BPMs used for calibration 2. The bunch angle effects corresponding to around 15 μm (the angle is around 100-200 μrad for the calibration data). 3. The resolution of the HOMBPM electronics. 4. The mechanical stability of the whole module including the BPMs.

As a comparison, calibration based on dipole signals in time domain gives an acceptable calibration RMS error (around 50 μm). However the RMS error for the validation datasets degrades over time to millimeter range. This motivated us to use dipole signal in the frequency domain for HOMBPM calibration.

4.4. Resolution

The minimum possible resolution, based on the thermal noise limit is no more than 130 nm [4]. The resolution of the HOMBPM is to a large extent limited by the resolution of the toroids (which contributes ~ 6 μm at a 1 mm offset) and the phase noise of local oscillator (which contributes ~ 1 μm at a 1 mm offset) [4]. We took multiple measurements of the charge and used the mean value. In this manner, we reduced the former effect. Using the spectra of dipole signals mitigates the phase issue.

The resolutions obtained are summarized Table 1. We achieved less than 2 μm resolution in the y direction for data from all dates based on the PLS method.

Table 1 Summary of resolution on January 23, 25 and May 1 based on three methods.

Dates \ Methods	PLS	SVD	ANN
January 25 (x, y) (μm)	(3.3, 1.5)	(4.1, 3.3)	(5.1, 3.0)
January 23 (x, y) (μm)	(2.5, 1.8)	(3.4, 4.4)	(3.8, 3.5)
May 1 (x, y) (μm)	(4.0, 1.7)	(4.5, 3.0)	(5.5, 2.7)

Note that in our study the resolution was evaluated within a beam position range of 2 by 2 mm^2. Therefore the resolution obtained is an averaged value within the range in contrast to the beam jitter data normally done for standard BPMs.

5. Summary and conclusions

The pre-processed datasets were used for calibration and validation of the HOMBPMs for the 1.3 GHz cavities in the 5^{th} accelerating module in FLASH. We used the RMS error as a figure of merit to evaluate and optimize the calibration. The resolution was calculated based on the three BPMs method.

Based on the analysis of dipole spectra instead of the time-based waveform, we consistently achieved a resolution better than 5 μm over a three month operational period. We used three methods to extract the beam position, namely ANN, SVD and PLS. The latter yielded the best resolution and minimum computation time.

Further work in this area will be focused on equipping the European XFEL [20] with HOM based diagnostics. Here a direct sampling of the waveforms will be used [21], and as a consequence we expect to have no issues with the local oscillator. This is expected to produce an enhanced resolution compared to the one reported here.

6. Acknowledgements

We are pleased to acknowledge helpful discussions with Thomas Wamsat and Bastian Lorbeer. We also appreciate the generous support received from the FLASH crew during the beam time. This work is supported partly by $EuCARD^2$, Grant Agreement 312453.

References

[1] Ackermann, W. et al. Operation of a free-electron laser from the extreme ultraviolet to the water window. *Nat. Photonics* 1; 2007, 336–342.
[2] Aune, B. et al. Superconducting TESLA cavities. *Phys.Rev.ST Accel.Beams* 3; 2000, 092001.
[3] Edwards, H. et al. 3.9 GHz Cavity Module for Linear Bunch Compression at FLASH. *Proc. LINAC10*; 2010, Tsukuba, Japan, p. 41.
[4] Molloy, S. et al. High precision superconducting cavity diagnostics with higher order mode measurements. *Phys.Rev.ST Accel.Beams* 9; 2006, 112802.
[5] Zhang, P. Beam Diagnostics in Superconducting Accelerating Cavities, Springer Theses. Springer International Publishing; 2013.
[6] Chao, A.W. *Physics of Collective Beam Instabilities in High Energy Accelerators*, New York: Wiley Series in Beam Physics and Accelerator Technology; 1993.
[7] Wangler, T.P. *RF Linear Accelerators*. Heppenheim: John Wiley & Sons; 2008.
[8] Wanzenberg, R. Monopole, Dipole and Quadrupole Passbands of the TESLA 9-cell Cavity, DESY Report: TESLA 2001-33.
[9] Jones, R.M. Wakefield suppression in high gradient linacs for lepton linear colliders, *Phys.Rev.ST Accel.Beams*; 2009, 12, 104801.
[10] Walston, S. et al. Performance of a High Resolution Cavity Beam Position Monitor System. *Nucl.Instrum.Meth*; 2007, A578, 1–22.
[11] Frisch, J. et al. Electronics and Algorithms for HOM Based Beam Diagnostics. *Proc. AIP Conf.*; 2006, 868, 313-324.
[12] Goloborodko, S. et al. DOOCS: an Object Oriented Control System as the integrating part for the TTF Linac. *Proc. ICALEPCS'97*; 1997, Beijing, China, p. 141.
[13] Shi, L. et al. Stability study of the higher order mode beam position monitors at the Accelerating cavities at FLASH. *Proc. IBIC14*; 2014, Monterey, CA, U.S.A., TUPF10.
[14] Zhang, P. et al. Statistical methods for transverse beam position diagnostics with higher order modes in third harmonic 3.9 GHz superconducting accelerating cavities at FLASH. *Nucl.Instrum.Meth*; 2014, A734, 84–94.
[15] Rosipal, R. et al. Overview and recent advances in partial least squares. in: Subspace, Latent Structure and Feature Selection Techniques, Lecture Notes in Computer Science, Springer; 2006.
[16] Battiti, R. First and Second-Order Methods for Learning: between Steepest Descent and Newton's Method. *Neural Comput*. 4; 1992, 141–166.
[17] Haykin, S.O., *Neural Networks and Learning Machines*. 3rd edition. New York: Prentice Hall; 2008.
[18] Anton, H. et al. *Elementary Linear Algebra: Applications Version*. 10th edition. New Jersey: Wiley, Hoboken, NJ; 2010.
[19] Narsky, I. et al. *Statistical Analysis Techniques in Particle Physics: Fits, Density Estimation and Supervised Learning*, 1st edition. Weinheim: Wiley-VCH Verlag GmbH & Co. KGaA; 2013.
[20] Altarelli, M. et al. (editors) The European X-Ray Free-Electron Laser-Technical Design Report. DESY Report: DESY 2006-097; 2006.
[21] Bou Habib, S. et al. New Design of High Order Modes Electronics in MTCA.4 Standard for FLASH and the European XFEL. *Proc. IBIC2013*; 2013, Oxford, UK, p. 443.